Two configurations of a channel-forming membrane protein

P. N. T. Unwin & P. D. Ennis

Department of Structural Biology, Stanford University School of Medicine, Stanford, California 94305, USA

The protein oligomer forming the gap junction channel has been analysed in two Ca^{2+}-sensitive states by electron microscopy of membranes in frozen aqueous solutions. Switching between states occurs by a small cooperative rearrangement involving tilting of the subunits, which may be responsible for the effect of Ca^{2+} on channel permeability in vivo.

FUNDAMENTAL biological processes such as the transmission of nerve impulses, visual excitation and cell-to-cell communication depend on the fact that membranes can regulate the passage of ions and/or small molecules across their surfaces. Proteins create channels in the membranes for this purpose and regulation is achieved by conformational changes of the protein in response to chemical or electrical stimuli. An example of such a protein is the one which forms the gap junction (or cell-to-cell) channel. We report here on its structure and action when stimulated by Ca^{2+}, an ion which induces this channel to close[1,2].

The protein is a cylindrical oligomer composed of six identical, rod-shaped subunits[3,4]. It spans the lipid bilayer, creating a channel along its central, hexad, axis. The channel traverses the plasma membranes of two apposed cells in consequence of a hexamer in one membrane being joined symmetrically to an oppositely facing hexamer in the other. These 12-subunit assemblies accumulate at specialized regions of contact (gap junctions), where they regulate the passage of small molecules and ions between cell interiors (reviewed in refs 5, 6).

Based on the appearance of gap junction surfaces in negative stain, we speculated that the channel might open and close, given the appropriate stimulus, by a coordinated tilting and sliding motion of the protein subunits along their lines of contact[4]. Subsequent X-ray diffraction experiments showed that a reversible transition of this nature could be induced by the action of Ca^{2+} *in vitro*[7]. Now we describe the two Ca^{2+}-sensitive configurations seen more directly in electron micrographs of junctions in frozen aqueous solutions. The three-dimensional maps obtained by this technique[8,9] reveal features of the subunits extending over their entire length, both within the lipid bilayer and in the aqueous spaces on either side. Differences between these maps demonstrate that Ca^{2+} does induce a small coordinated rearrangement of the subunits around the channel and affect its dimensions in a manner consistent with the original proposal.

Imaging and diffraction

We made one preparation of rat liver junctions for these experiments and produced two alternative structures by dialysing separate portions against Ca^{2+}-free (5 mM EGTA, 0.5 mM $MgCl_2$, 5 mM HEPES *p*H 8.0) and Ca^{2+}-containing (0.05 mM $CaCl_2$, 5 mM HEPES *p*H 8.0) solutions. Methods were as described previously[7]. Such junctions are double membrane plaques, 0.5–1.5 μm in diameter, composed of ordered domains of oppositely facing hexamers and intervening lipid molecules. The hexamers pack within the domains on a hexagonal lattice of dimension 80–85 Å and protrude into the space between the two membranes, making a gap between them of ~30 Å.

Electron microscopy was used to derive a set of three-dimensional Fourier terms corresponding to each structure. The junctions were frozen in their respective solutions and examined with a cold stage at −120 °C. Images were recorded of specimens tilted at angles of up to 53° to the incident 100-kV electron beam (Fig. 1). Densitometry and computer processing were carried out as described previously[4,10] and the Fourier terms to 20 Å resolution from each image were combined according to the symmetry of the space group P6. The average phase errors in combining the data were 16.7° and 15° for the $-Ca^{2+}$ and $+Ca^{2+}$ structures, respectively, based on comparisons between each new phase and all previously accumulated values related by symmetry. For both structures, 18 images provided sufficient values of amplitude and phase to map out the continuous variations along each of the five crystallographically independent reciprocal lattice lines. Curves were fitted to the data along the lattice lines by a least-squares method[11], with the amplitude curves weighted according to the reliability of the corresponding phases (Fig. 2). These curves, sampled at regular intervals (0.002 $Å^{-1}$), provided the Fourier terms for calculating three-dimensional maps.

There were cones of missing information due to the restricted ranges of tilt. By far the most significant omissions, according to X rays[7], were the terms from the central (0, 0) lattice line. These terms determine only the absolute levels of the contours in sections parallel to the membrane and therefore have no influence on the positions of peaks identifying the paths taken by the protein subunits, described below. They do, however, affect the dimensions of features bound by shallow gradients, for example the channel. Such dimensions were obtained more accurately previously[4] with complete sets of Fourier terms.

X-ray diffraction was used (as in ref. 7) to provide an independent evaluation of the structures. The partially oriented gap junction pellets gave rise to intensities along the lattice lines which were smeared into concentric arcs. Traces across these arcs, obtained by circular integration, were very similar to analogous profiles calculated from the electron microscopic data (Fig. 2, panel 6). Moreover, in comparing the two structures,

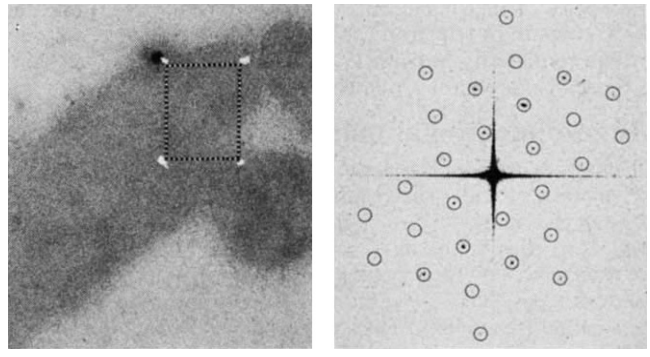

Fig. 1 Image (×32,000) and optical diffraction pattern (from the boxed area) of a gap junction frozen in Ca^{2+}-free solution and tilted 31.5° to the incident electron beam. The regular hexagonal lattice is evident from the array of diffraction peaks encircled, but is barely visible in the image because of the small differences in electron scattering properties between ice, lipid and protein.

0028-0836/84/070609—05$01.00

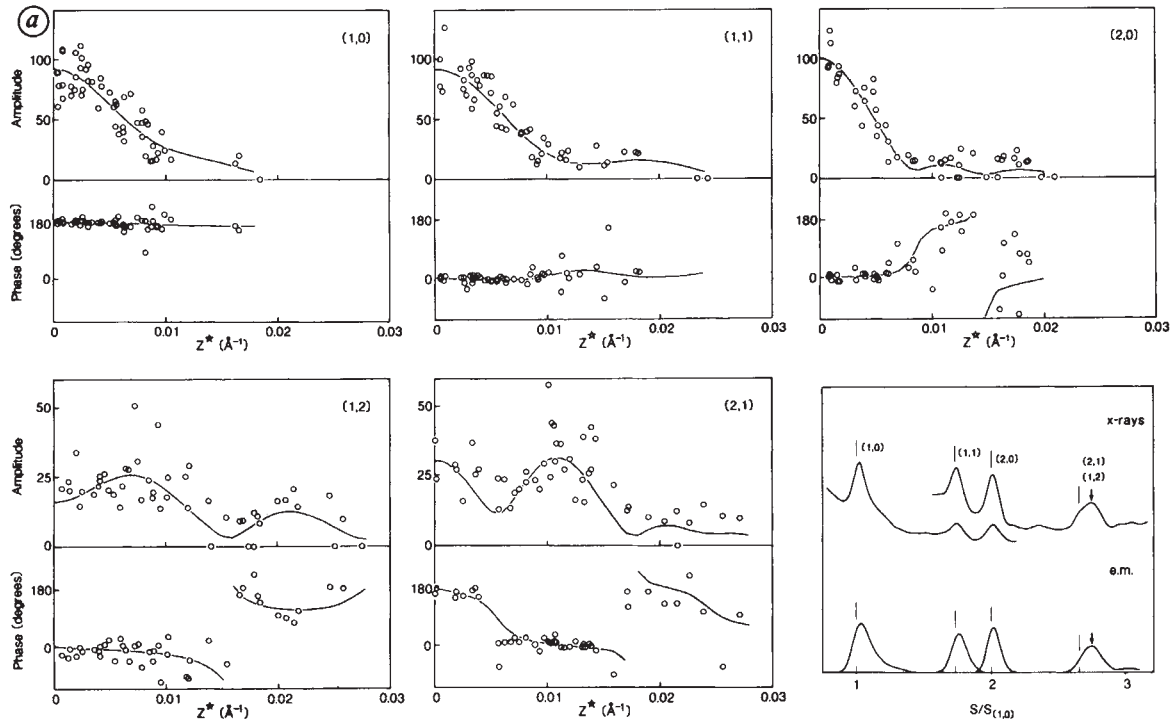

Fig. 2 Diffraction data from gap junctions in: *a*, Ca^{2+}-free solution; *b* (right), Ca^{2+}-containing solution. The values of amplitude and phase along the reciprocal lattice lines (first five panels) were derived from images of junctions tilted to the incident electron beam by angles of up to 53° in *a* and 50° in *b*. Z^* is the distance from the midpoint along the lattice line; the Friedel relationship gives the values for negative Z^*. The sixth panel shows X-ray traces.

Methods: Specimens were prepared by the double carbon film technique[8,20]. The carbon support grid containing the junctions was immersed in 10× diluted Ca^{2+}-free or Ca^{2+}-containing solution, raised through a second carbon film floated on the surface, pressed firmly onto Millipore filter paper, held away from the filter paper for several seconds and then plunged into liquid nitrogen. Holes in the support film were important for efficient withdrawal of excess solution onto the filter paper. After transfer to the microscope, the grids were maintained at ~−120 °C using a modified Philips EM300 high-resolution stage[21]. Images were focused using an off-axis viewing screen[22], and recorded at a magnification of ×28,000 on Kodak 4463 film with low doses (2–5 electrons Å^2) to minimize radiation damage. Films were developed in full strength Kodak D19 developer for 8 min. Tilting was accomplished by bending the microscope grids under liquid nitrogen before inserting them into the stage. Preliminary selection of images was by optical diffraction evaluation of the strength of the Fourier terms and of the focus levels indicated by the positions of the zeros between the Thon rings[19]. Images only gave suitable diffraction patterns if they were of specimens surrounded by visible films of ice. Those images selected for subsequent processing and incorporation into the three-dimensional data sets all had underfocus values within the range: 4,000–12,000 Å; thus, variations in strengths of the Fourier terms due to different contrast transfer functions were small. In the processing, the densitometer step and sampling sizes were 20 μm, equivalent to 7 Å at the specimen, and the array size for Fourier transformation was 512×512. An analysis of images very close to focus indicated that the poorer contrast transfer at low spatial frequencies, produced by underfocusing, weakened the amplitude of the (1, 0) peak by up to 30% relative to values for the other peaks; the same correction was applied to all images for this effect. Tilt angles and axes were estimated from the geometry of the peaks in the computed Fourier transforms and from focus changes across the film. In combining the Fourier terms from different images, the comparison range used along Z^* was 0.0022 Å^{-1}. Images were not incorporated into the three-dimensional data sets if the phase residuals, based on comparisons with the previously accumulated phases, were greater than 25°. With specimens tilted by >45°, some of the terms were omitted from the refinement. Unlike previously[4], junctions from this preparation were strongly chiral (see also ref. 23), a feature most obvious from the opposite phases of the (1, 2) and (2, 1) peaks at low values of Z^*. Seven of the 18 images for *a* and 8 of the 18 images for *b* were of junctions with their positive crystallographic direction pointing towards the electron source. The X-ray traces (panel 6) were obtained from partially oriented pellets, as described previously[7]. The dimensionless parameter, $S/S_{(1,0)}$, provides a linear reciprocal scale such that the hexagonal lattice positions, marked by vertical lines, are at 1, $\sqrt{3}$, 2 and $\sqrt{7}$. Peak values depart from these positions depending on the strength of the Fourier terms along the lattice lines away from the point, $Z^* = 0$. The electron microscopy-derived curves compared were obtained by plotting the amplitudes against reciprocal spacing, rather than Z^*, squaring to obtain intensities and convolving these intensities with a gaussian distribution to simulate the broadening of the X-ray peaks due to finite beam size and disorder. Changes in the position of the overlapped (2, 1) and (1, 2) peak (arrows) and in the intensity of the (1, 0) peak represent the most significant differences between the two structures. These changes are consistently observed in the X-ray patterns[7].

the same differences (displacement of the overlapped (2, 1) and (1, 2) peak; change in intensity of the (1, 0) peak) were indicated by X rays as by electrons. Therefore, we presume that the protein configurations being visualized at −120 °C are the same as those at more natural temperatures.

Three-dimensional maps

The maps, synthesized from the two sets of Fourier terms, depict the protein subunits surrounding the channels and extending through the lipid bilayer into the aqueous spaces on either side (Fig. 3). The subunits have several features of interest. They are rods which in cross-section must taper significantly towards the hexad axis. They are tilted tangentially and radially around the channel (see below). They appear more distinct and slightly thicker in the bilayer than in the extracellular region, as if their secondary structures in the two environments are quite different.

Ice and lipid are not separately resolved because of their similar mean electron scattering densities. Thus, the maps do not reveal accurately the extents to which the subunits protrude from the bilayer. However, the surface details seen with negative stain[4] correspond to features in Fig. 3 and suggest that the subunits protrude from the bilayer only slightly on the cytoplasmic side (5–10 Å) compared with the extracellular side (15–20 Å).

The hexamers come closest to each other inside the bilayer and the way they fit into the crystalline lattice depends on the bilayer in question. In Fig. 3 the ridges on the sides of the hexamers interlock, forming the same neighbour-to-neighbour relationship in both maps, while in the other bilayer they abut. The latter hexamers are less well preserved, and probably distorted, as the density fluctuations associated with their subunits are weaker (by 45% and 15% for the $-Ca^{2+}$ and $+Ca^{2+}$ structures, respectively). These effects may reflect constraints on the potentially more open packing due to the restricted volume of lipid present or due to the curved membranes of isolated junctions[12] being forced to lie flat. More symmetrical packing[4] presumably occurs when more lipid is available to fill intervening spaces.

Differences

The hexamers look different in the two maps because of the different subunit configurations. They also have a slightly smaller

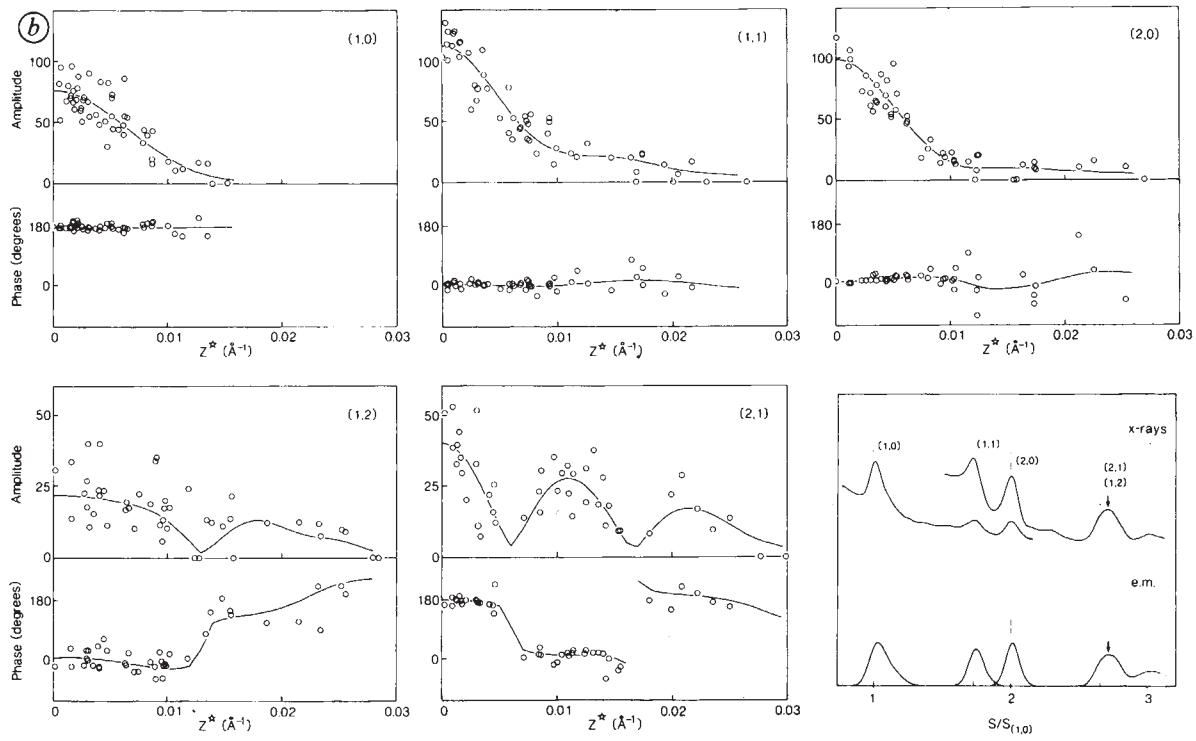

diameter in the $+Ca^{2+}$ structure, where the lattice dimension is almost 2 Å less[7]. We analysed the differences by comparing the tangential and the radial displacements of the peaks around the channel at various levels through the two structures. In projection down the hexad axis (Fig. 4) these peaks follow curved paths which are more foreshortened for the $+Ca^{2+}$ than for the $-Ca^{2+}$ subunits. The $+Ca^{2+}$ subunits, then, are aligned more nearly parallel to the hexad axis. From the direction and magnitude of foreshortening we find that the two paths of the subunits are related, approximately, by a tilt of ~7.5° tangential to the hexad axis and about the extracellular end (compare Fig. 4*b* and *c*).

The radial path changes of the subunits in going to the $+Ca^{2+}$ configuration are small: about 2 Å inwards towards the cytoplasmic end, but outwards towards the extracellular end (Fig. 5). As shown, the constricting action at the cytoplasmic end would be expected from a tilt strictly tangential to the hexad axis. However, the opposite action at the other end is an additional feature, increasing slightly the separation between neighbouring subunits in the part of the structure outside the cell. This could be needed for the subunits to fit into the 'tighter' configuration without being deformed.

The significance of the small radial changes was checked by calculating difference Fourier maps between the two structures. In these maps the displacement of matter into and away from the channel is seen as two peaks of opposite sign, centred on the hexad axis and near the two ends of the subunits. The peaks were present in both membranes and did not depend on which way up one structure was with respect to the other. Further, the major difference terms responsible for the peaks were significant at the 5% level, based on the standard deviations of the observed amplitudes along the contributing reciprocal lattice lines.

Switching between the two structures

The three-dimensional maps revealed several basic features of this channel-forming protein, It has a length of ~70 Å perpendicular to the plane of the membrane and an average diameter of ~64 Å within this plane. It occupies a space of ~225,000 $Å^3$ (from the zero-level contour), consistent with the value estimated from the subunit molecular weight, 28,000 daltons (refs 13, 14), assuming 1.3 $Å^3$ per dalton for the partial specific volume. It is composed of two main portions, one within and the other outside the membrane, which differ distinctly in

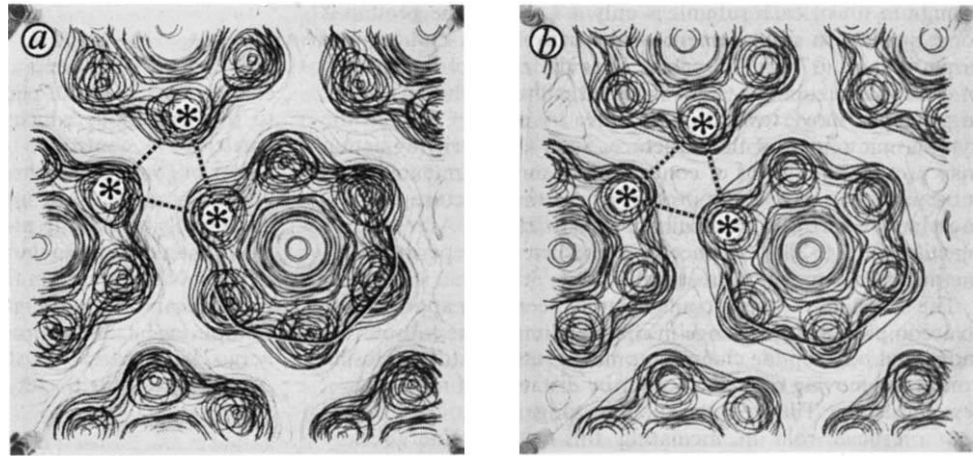

Fig. 3 Maps of the $-Ca^{2+}$ (*a*) and $+Ca^{2+}$ (*b*) structures in one of the membranes, as they would appear viewed from the inside of the cell. The distance between channels in *a* is 82.4 Å and in *b* it is 80.6 Å, from X rays[7]. The six surrounding protein subunits create strong fluctuations in density within the lipid bilayer, but weaker fluctuations in the aqueous extracellular space (furthermost portion of hexamer, outer surface partly outlined). All hexamers have the same neighbour-to-neighbour relationship where they come closest to each other, near the middle of the bilayer (indicated by equivalent triangles connecting equivalent points in the two maps). The positive and zero-level contours (darker) correspond to regions of higher electron scattering density. Detail extends over a distance of 68 Å perpendicular to the sections; fluctuations in density outside the maps on the cytoplasmic side are less than one contour level.

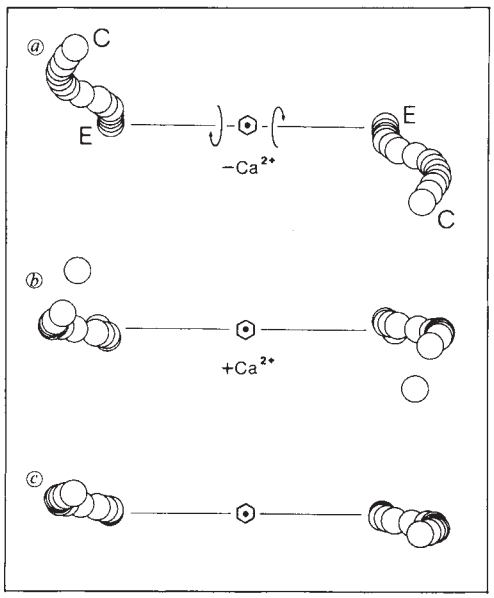

Fig. 4 Projection down the hexad axis of paths taken by subunits on opposite sides of the channel: *a*, $-Ca^{2+}$ and *b*, $+Ca^{2+}$ structures; *c*, path derived from *a* assuming a tilt of 7.5° about the radial axis is indicated. The circles mark the peak positions in sections parallel to the membrane through the three-dimensional maps. E and C are the extracellular and cytoplasmic ends of the subunits, respectively, corresponding to the top and bottom sections in Fig. 3. Correspondence between *c* and *b* indicates that the paths in *a* and *b* are related, approximately, by a small tilt tangential to the hexad axis.

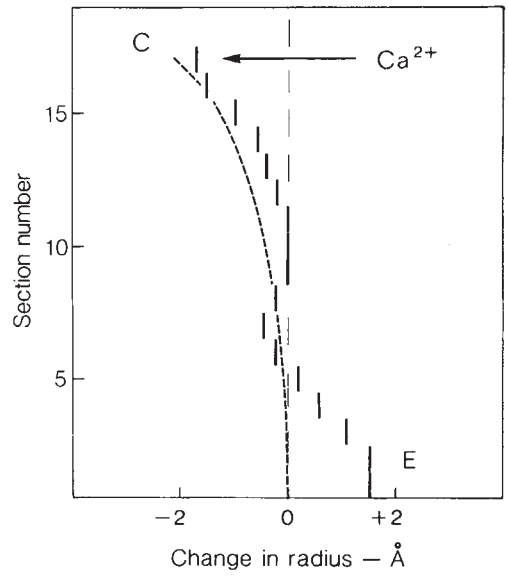

Fig. 5 Radial displacements of the subunits relative to the hexad axis (vertical) on addition of Ca^{2+}, determined from the positions of peaks around the channel in sections through the three-dimensional maps. The broken line shows the radial displacement corresponding to the tilt *a* to *c* in Fig. 4. E and C are as in Fig. 4. Similar radial displacements are suggested by the negative stain maps (ref. 4, Fig. 4), which show a decrease and an increase in stain accumulation in the cytoplasmic and extracellular parts of the channel, respectively.

appearance. In detail, the structure appears rather different from that determined from mouse liver gap junctions[3,12].

Calcium acts to produce small variations in these features by changing, or switching, the configurations of the subunits. From the differences in configuration investigated above, the switch must entail motion of essentially rigid rods having surfaces which do not rotate about the rod axes, but continue to point in the same directions. At low resolution, therefore, it consists simply of a rearrangement of the subunits by tilting and sliding along their lines of contact. This observed mechanism by which the protein changes its structure confirms the one proposed[4], based on the appearance of gap junction surfaces in negative stain.

What is the effect of calcium on the dimensions of the channel? The rearrangement is depicted by wooden models (Fig. 6). We found that subunits on either side of the channel become aligned more nearly parallel to it on exposure to Ca^{2+}. They tilt in opposite senses about a radial axis at the extracellular end (bottom of model) and consequently are displaced tangentially towards each other at the cytoplasmic end (top of model). The change in tilt of each subunit is only ~7.5°, but the protein is long, so that its displacement at the cytoplasmic end is quite large, that is, $\sim 70 \sin 7.5 = 9$ Å. Thus the channel-lining faces of each pair of subunits (not visualized at this resolution) could, in principle, move towards each other by up to ~18 Å in the cytoplasmic region of the structure. Such a constricting action may provide the means of controlling channel permeability, as it occurs in the part of the protein where the structure changes most and where the channel appears to close[4]. A restrictive opening of 16–20 Å diameter is predicted by permeability measurements made on mammalian cells[15,16].

The switching between configurations seen here appears able to accomplish a large change in channel dimensions without the individual polypeptide chains becoming grossly distorted, losing contact or moving over each other by distances of more than a few angstroms. Tilting of the subunits tangential to the channel has a crucial role in mediating this action. Energetically unfavourable interactions are avoided by the subunits moving predominantly parallel to the plane of the bilayer and keeping the same polar and hydrophobic surfaces exposed to the solvent

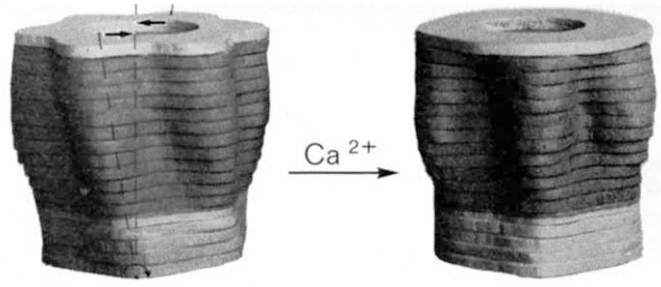

Fig. 6 Models of the two protein configurations, constructed from the maps in Fig. 3. The lighter shaded portions correspond to parts of the protein contacting fluid inside (top) and outside (bottom) the cell; the darker shaded portion would be in contact with lipid. The configurations are related to each other by tilt axes passing radially through the bases of the subunits (as depicted on the left-hand model). Subunits on either side of the channel tilt in opposite directions about these axes, and the resulting tangential displacements (pair of arrows) are greatest at the upper, cytoplasmic face.

and lipid. It is a cooperative mechanism, as the subunits must change their mode of packing together, and may be analogous to the transitions which occur in spherical and helical virus particles[17,18], controlled by divalent cation concentration or *p*H. Other oligomeric membrane proteins may respond to chemical or electrical stimuli by undergoing similar rearrangements predominantly within the plane of the bilayer.

We thank Chris Raeburn for constructing the electron microscope cold stage used in this work. We also thank David Agard, David Grano, Ron Milligan and Guido Zampighi for their help. Computing facilities were generously provided by Dr L. Herzenberg. The research was supported by grants from the NIH and American Cancer Society.

Received 27 June; accepted 31 October 1983.

1. Rose, B. & Loewenstein, W. R. *Nature* **254,** 250–252 (1975).
2. Spray, D. C., Stern, J. H., Harris, A. L. & Bennett, M. V. L. *Proc. natn. Acad. Sci. U.S.A.* **79,** 441–445 (1981).

3. Makowski, L., Caspar, D. L. D., Phillips, W. C. & Goodenough, D. A. *J. Cell Biol.* **74,** 629–645 (1977).
4. Unwin, P. N. T. & Zampighi, G. *Nature* **283,** 545–549 (1980).
5. Hertzberg, E. G., Lawrence, T. S. & Gilula, N. B. *A. Rev. Physiol.* **43,** 479–491 (1981).
6. Loewenstein, W. R. *Physiol. Rev.* **61,** 829–913 (1981).
7. Unwin, P. N. T. & Ennis, P. D. *J. Cell Biol.* **97,** 1459–1466 (1983).
8. Taylor, K. A. & Glaeser, R. M. *Science* **186,** 1036–1037 (1974).
9. Dubochet, J., Lepault, J., Freeman, R., Berriman, J. A. & Homo, J.-C. *J. Microsc.* **128,** 219–237 (1982).
10. Henderson, R. & Unwin, P. N. T. *Nature* **257,** 28–32 (1975).
11. Agard, D. A. *J. molec. Biol.* **167,** 849–852 (1983).
12. Caspar, D. L. D., Goodenough, D. A., Makowski, L. & Phillips, W. C. *J. Cell Biol.* **74,** 605–628 (1977).
13. Hertzberg, E. L. & Gilula, N. B. *J. biol. Chem.* **254,** 2138–2147 (1979).
14. Nicholson, B. J., Hunkapiller, M. W., Grim, L. B., Hood, L. E. & Revel, J.-P. *Proc. natn. Acad. Sci. U.S.A.* **78,** 7594–7598 (1981).
15. Flagg-Newton, J., Simpson, I. & Loewenstein, W. R. *Science* **205,** 404–407 (1979).
16. Schwarzmann, G. *et al. Science* **213,** 551–553 (1981).
17. Durham, A. C. H. & Klug, A. *Nature new Biol.* **229,** 6–10 (1971).
18. Robinson, I. K. & Harrison, S. C. *Nature* **297,** 563–568 (1982).
19. Thon, F. *Z. Naturforsch.* **219,** 476–478 (1966).
20. Jaffe, J. & Glaeser, R. M. *Proc. 40th an. EMSA Meet.*, 72–73 (San Francisco, 1982).
21. Taylor, K. A., Milligan, R. A., Raeburn, C. & Unwin, P. N. T. *Ultramicroscopy* (submitted).
22. Unwin, P. N. T. & Henderson, R. *J. molec. Biol.* **95,** 425–440 (1975).
23. Baker, T. S., Caspar, D. L. D., Hollingshead, C. J. & Goodenough, D. A. *J. Cell Biol.* **96,** 204–216 (1983).

LETTERS TO NATURE

Implications of 10^{16} eV γ rays from Cyg X-3

David Eichler

Astronomy Program, University of Maryland, College Park, Maryland 20742, USA

W. Thomas Vestrand

Physics Department, University of New Hampshire, Durham, New Hampshire 03824, USA

Samorski and Stamm[1] have reported and Lloyd-Evans *et al.*[2] have recently confirmed the detection of high-energy quanta, presumably γ rays, with energies $E > 2\times10^{15}$ eV from Cygnus X-3. These ultra-high energy (UHE) γ rays were detected with extensive air shower arrays and included four events with $E > 10^{16}$ eV. Temporal analyses[1,2] of the events indicate that the flux is modulated with a 4.8-h period and is sharply pulsed. Here (1) we discuss the implications of these γ-ray detections and suggest that autocorrelating the air shower data may be the best way to determine the intrinsic width of the γ-ray pulses; (2) we argue that the radiating particles are accelerated by a pulsar and that if they are accelerated according to any pulsar mechanism we know of, then they must be ions; (3) we note that if the ions are accelerated to 10^{16} eV by a large amplitude Deutsch wave, then the gravitational wave luminosity L_g should exceed that of the Crab pulsar by a factor of $\sim5\times10^5$, and the spin-down time should be ~80 yr (requiring a truly remarkable object); and (4) we show that the ions can be accelerated in the near zone but only if, contrary to the standard view, pair production does not greatly reduce the vacuum potential drop in the near zone. We note that near-zone acceleration could be confirmed by detection of curvature radiation.

Several groups have detected γ rays from the Cyg X-3 system at energies $<10^{15}$ eV using atmospheric Cerenkov techniques. The system is known to be a luminous ($L_{peak} > 10^{37}$ erg s^{-1}) source of TeV γ rays[3–5]. The flux at TeV energies is periodic and has the same 4.8-h periodicity seen in medium energy γ rays[6] (~10^2 MeV), X rays[7], and at IR energies[8] and is generally identified as the orbital period. The TeV light curve is composed of two narrow pulses separated by ~1.9 h (ref. 3), and roughly centred about the X-ray minimum. A possible detection of γ rays having energies in the range 10^{14}–10^{15} eV is reported by Bhat *et al.*[9], who studied the arrival times of atmospheric Cerenkov pulses produced by air showers with energies $E > 10^{14}$ eV. By autocorrelating their data they found a significant excess of events with time separations $\Delta t < 40$ s that had a sidereal association. The width of the directional enhancement peak in right ascension is comparable to the angular response function of the detection system. Their data is consistent with a point source at a right ascension of 20 ± 1 h. The detection system was stationed at Gulmarg, India (latitude 34° N) and pointed at the zenith. It is tempting to identify this nonrandom air shower component with γ rays from Cyg X-3 ($\alpha = 20$ h 31 min, $\delta = 40°\,47'$). However, the required flux would have to be roughly a factor of three larger than the upper limit of Fegan and Danaher[10] and several orders of magnitude higher than the value obtained by interpolating between measurements at 10^{15} eV and below 10^{13} eV. Nevertheless, we feel that autocorrelating the data may be the best way to determine the intrinsic width of the γ-ray pulses since small errors in the ephemeris will broaden pulses in phase histograms that are generated using data obtained over long periods of time. Taken at face value, the observations of Bhat *et al.*[9] indicate an excess only for $\Delta t < 40$ s (the autocorrelation was done only up to $\Delta t = 450$ s) and require the pulses to be extremely narrow ($\Delta\phi = 2\times10^{-3}$). We feel that an autocorrelation analysis of data obtained by a detection system with better angular resolution could be useful for determining whether or not the pulses are actually this narrow.

A natural interpretation of the narrow pulses is that Cyg X-3 is a young pulsar in a binary system[11] that is emitting UHE particles which interact with the corona of the companion star[12]. Most of the UHE emission should come from a translucent 'window' (optical depth $\tau \sim 1$) in the companion star's corona, which may be extremely variable and complex due to its interaction with the pulsar wind. Higher τ would obscure the photons, and lower τ would be inefficient as a scintillation screen. It seems reasonable that the translucency condition is fulfilled, during any given orbital period, for 40 s which would account for the autocorrelation time scale. If the pulse width is actually this narrow, the intrinsic luminosity of the system must be $L > 1.3\times10^{39}$ erg s^{-1}; this would rank the pulsar as the youngest known.

The production of γ rays with $E > 10^{16}$ eV requires, of course, the acceleration of particles to even higher energies. We have argued elsewhere[12] that shock-accelerated particles could not generate narrow γ-ray pulses at energies $E > 10^{14}$ eV. The basic point is that shock acceleration requires scattering, whereas the narrow pulses at the observed phases imply straight-line trajectories. Additional arguments rule out shock acceleration of electrons beyond $\sim10^{14}$ eV (ref. 12).

We now consider whether acceleration by a large amplitude Deutsch wave, as proposed by Gunn and Ostriker[13], could account for particles whose energy exceeds 10^{16} eV. The maximum energy that a particle with mass Am_p and charge Ze can attain by this mechanism is

$$E_{max} \simeq 6\times10^{14} A^{1/3} Z^{2/3} \times \left(\frac{B_{surf}}{10^{12}\,G}\right)^{2/3} \left(\frac{P}{10\,ms}\right)^{-4/3} \left[\ln\left(\frac{R_B}{R_L}\right)\right]^{2/3} \quad eV \quad (1)$$

where B_{surf} is the surface magnetic field, P is the pulsar's period, and R_L and R_B are the radii of the light cylinder and binary orbit, respectively. The luminosity in magnetic dipole radiation would be (magnetic moment assumed $\perp$ to $\vec{\Omega}$):

$$L_{MD} \simeq 6.5\times10^{40} \left(\frac{P}{10\,ms}\right)^{-4} \left(\frac{B_{surf}}{10^{12}\,G}\right)^{2} \quad erg\,s^{-1} \quad (2)$$

0028–0836/84/070613—02$01.00